IJCRT.ORG ISSN : 2320-2882

INTERNATIONAL JOURNAL OF CREATIVE RESEARCH THOUGHTS (IJCRT)

An International Open Access, Peer-reviewed, Refereed Journal

FLUID DYNAMICS BASED MATHEMATICAL BOUNDARY LAYER THICKNESS ANALYSIS ON PROPERTIES OF BOUNDARY-LAYER FLAT PLATE CONFIGURATIONS

Jella Suman, Research scholar, Department of mathematics, Osmania university Telangana India

Prof J.Anand Rao. HOD of mathematics Department Osmania University, Telangana India

ABSTRACT:

The asymptotic limit of fluid flow at zero viscosity is a major issue in mathematical fluid dynamics analysis. This is especially true when there are boundaries present, since boundary layer separation often results in the generation of vorticity at the boundary. The analyzed real-world geometries were representative of a turbine rear frame's regular vanes and mount vanes. Bumpy vanes have been compared to a flat plate in order to determine the effect of bumps on the boundary layer and whether it is possible to compare the results to those from a flat plate. To measure the suction peak boundary layer thickness, we used the regular vane and the mount vane. It was discovered that the method used to estimate the thickness of the boundary layer is unreliable in cases where the flow over the vane separates. 1 mm bumps located at 32 percent of the nominal boundary layer thickness on the regular vane and 30 percent on the mount vane has no separation. Flat plate results differ from the boundary layer thickness increase and a detailed analysis of how the thickness is calculated must be performed. 1mm bumps were used to measure correlation, with a 0.285 drag coefficient for the regular vane and 0.275 for its mount version. Using a different method and similar geometry, the department came up with a drag coefficient of 0.25%, which can be used to compare. XFOIL has been used to investigate the properties of the boundary layer over a flat plate, both analytically, experimentally, and numerically. Analysis of the boundary-layer properties over an infinitesimal thin flat plate has been carried out using the theory of Blasius and von Karma. An aerodynamically flat plate with a Hermite polynomial leading edge and a trailing edge that corresponds to the last 70% of a NACA 4-series airfoil section has been analysed with XFOIL and tested in the Silent Wind Tunnel of the University of Twente.

1. INTRODUCTION

Mathematically well defined displacement thickness and its related momentum thickness appear to be more popular than descriptions of the boundary layer region. It is true, however, that these parameters are not very useful for describing, visualising, and/or conceptualising the behaviour of the boundary layer velocity profile. A similar problem exists when attempting to characterise the thermal boundary layer.

Following, we introduce a number of additional parameters that are useful in describing the behaviour of velocity and thermal boundary layers, as well as the thickness of the boundary layer. Laminar flow over a plate at zero incidence angle results in a Gaussian-like behaviour for both parallel flow velocity and temperature second-derivatives at zero incidence angle. Probability distribution function theory is used to explain the boundary layers of velocity and temperature as moments in second derivative kernels of the velocity and temperature profiles.

1.1 Background

To develop and produce components for commercial and military aircraft engines, VAC collaborates with some of the world's most renowned engine makers. GE, Pratt & Whitney, and Rolls-Royce are just a few examples. Because of this, VACs components can be found in 90 % of the world's large commercial aircrafts. The motto, "Make It Light" is the core in VACs goal to reduce aircraft emissions by 50 % until 2020, and the company focuses heavily on developing lightweight solutions for aircraft engine structures and rotors. Within the areas of specialization for commercial components (Figure 1) Volvo has established a number of Centers of Excellence (CoE) and Advanced Technology Areas, which have enabled them to focus on developing optimal advanced technology solutions and being able to provide strong competence in all engineering disciplines.

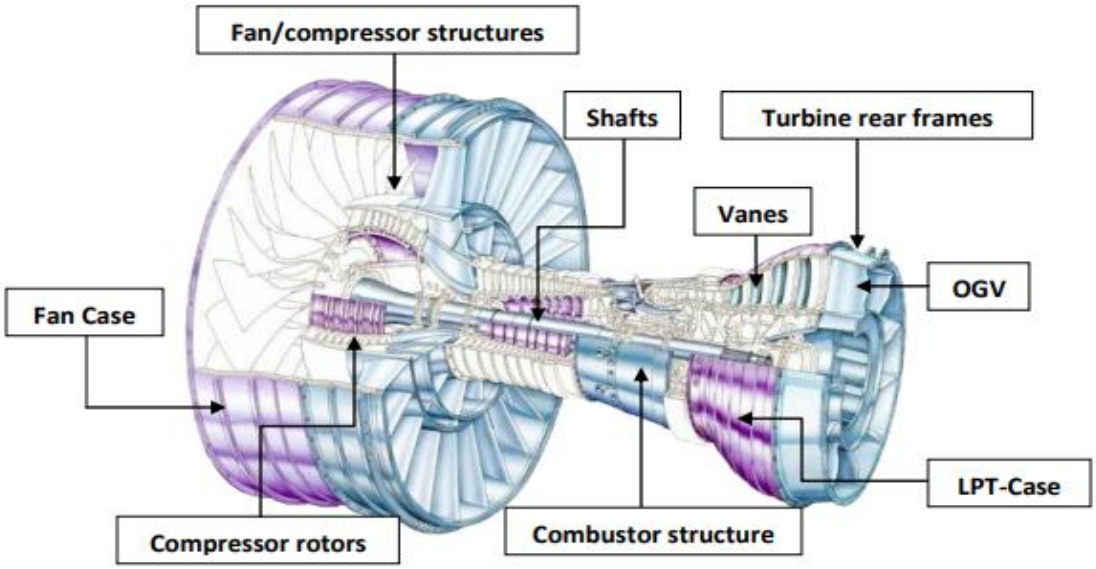

Figure 1: Some of the components of a jet engine and also Volvo Aero's commercial component specializations.

This project has been conducted in one of these CoEs, namely the aero-thermodynamics department, which is the competence centre for method and technology development within aerodynamics at VAC. Aero acoustics and aeromechanics, combustion, heat transfer, radiation, performance, and experimental verification are a few of the many fields in which this function is utilised throughout the product development process.

1.1.1 Non-conformance definitions

During manufacturing, the engine components go through a number of processes, like assembly and adjustment which will affect the products in different ways. This quite often has the impact that the finished product does not look like the intended design. The difference between the nominal (ideal) design of the components and the actual finished products is what causes non-conformances (NCs) or geometry defects. These deviations can have an unfortunate impact on the engine performance resulting in e.g. increased pressure losses, flow separation and increased swirl angles. The challenge is to determine how much these NC affects the aerodynamics of the components and if it is possible to relieve manufacturing and design constraints if they are found not to be detrimental. It will then be possible to reduce manufacturing and design costs.

1.2 Purpose of the project

It is thus of great interest for the department to know if the definitions can be considered accurate enough or if they need to be adjusted. Therefore, one of the purposes of this project is to validate the defined borders of the local defects to see if the definitions needs to be adjusted or not. The second purpose is to develop a correlation for calculating the drag coefficient of a bump, consisting of variables such as bump height in relation to boundary layer thickness and the Reynolds number at the bump position. The correlation can then be used in a non-conformance analysis program currently in development at the department.

2. GENERAL APPROACH FOR FLOWS WITH VORTICITY

Due to fluid viscosity, flow vortices in the boundary layer are significantly non-uniform. Between zero and some value on the body boundary, the vorticity changes as a function of distance from the boundary. In order to account for the non-uniformity of the vorticity, discrete vortex sheets are used instead of continuously distributed vorticity in the flow region. There is no vortexing between vortex lines, and the sheets of vortexing are arranged along the flow. As depicted in Figure 2, vortex sheets or streamlines separate the flow region into layers/channels. The normal and tangential components of the velocity and pressure in the channels are both continuous, but their tangential components are not. The velocity profile gradually changes from one channel to the next when using this technique. As the number of layers/channels increases, the stepwise discontinuity in the velocity profile disappears, and this is true up to an infinite number of layers/channels. The original flow's non-uniform vorticity can be seen here.

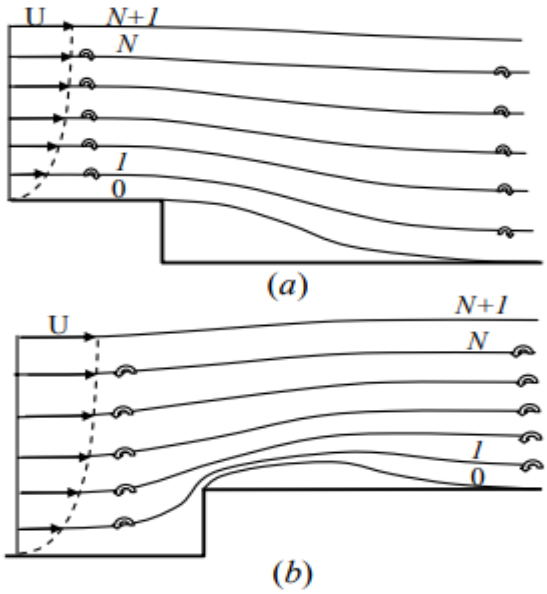

Figure 2. Sketch of a vortex flow: (a) past a downward step. (b) past an upward step.

The theory of potential flows can be used to solve the cavity flow problem with vorticity using this vortex flow model. First, the problem is a cavity flow in a finite-width channel with a specified lower-side shape and an upper-side velocity distribution (see Figure 2); the second type is a channel flow with curved walls (see Channels 1 N); the third type is a semi-infinite surface flow (see Layer N + 1), which is described in detail in the following sections. The original problem is made up of these three types of vortex-free problems.

Complex velocity and complex potential derivatives can be formulated as boundary value problems on the parameter plane introduced by them. Using these functions, the physical-to-parameter mapping function can be determined as follows:

$$z(\zeta) = z_o + \int_0^{\zeta} \frac{dz}{d\zeta}\, d\zeta$$

$$= z_o + \int_0^{\zeta} \frac{dw}{d\zeta} \Big/ \frac{dw}{dz}\, d\zeta \quad (1)$$

where z_o is the point in the physical plane corresponding to the point $\zeta = 0$ in the parameter plane.

The following is a list of the problems that have been solved so far. Solution of this problem, as shown in Figure 2, yields an upper-wall shape based on previous iteration's velocity magnitude assumption, as shown in this figure. In channel 1, the lower side of this wall is considered to be a solid wall. It is assumed that velocity magnitude along channel 1's upper wall is already known from previous iterations. The shape of channel 1's upper side can be determined by solving the problem. N + 1 is the half-space of the liquid that flows along the curved solid wall of the channel N by repeating the process. Solving this problem gives us information about the upper wall velocity of channel N.

Based on the observation that, except for around $\eta = 0$, the resulting profile is well approximated by a Gaussian curve when plotting f''' versus η this method for defining the boundary layer was developed. There are two ways to check for Gaussian-like behaviour: the second derivative plot and a least squares fit to that plot. Instead, we'll take a different route because it's more instructive than the one we're currently on. Due to the second derivatives' gaussian behaviour, it is possible to approximate the velocity profile as the integral of the integral of a Gaussian. The approximate expression for velocity based on the Gaussian-Error function is as follows:

$$\frac{u(y)}{U_\infty} \cong \frac{\sqrt{2}\sigma_v}{s\mu_1\sqrt{\pi}}\left[EXP\left(-\frac{1}{2}\left({}^{\mu_1}/_{\sigma_v}\right)^2\right) - EXP\left(-\frac{1}{2}\left(\frac{y-\mu_1}{\sigma_v}\right)^2\right)\right] + \frac{y}{s\mu_1}\left[1 - ERF\left(\frac{\sqrt{2}}{2}\left(\frac{y-\mu_1}{\sigma_v}\right)\right) + \frac{1}{s}\left[ERF\left(\frac{\sqrt{2}\mu_1}{2\sigma_v}\right) + ERF\left(\frac{\sqrt{2}}{2}\left(\frac{y-\mu_1}{\sigma_v}\right)\right)\right]\right] \quad (2)$$

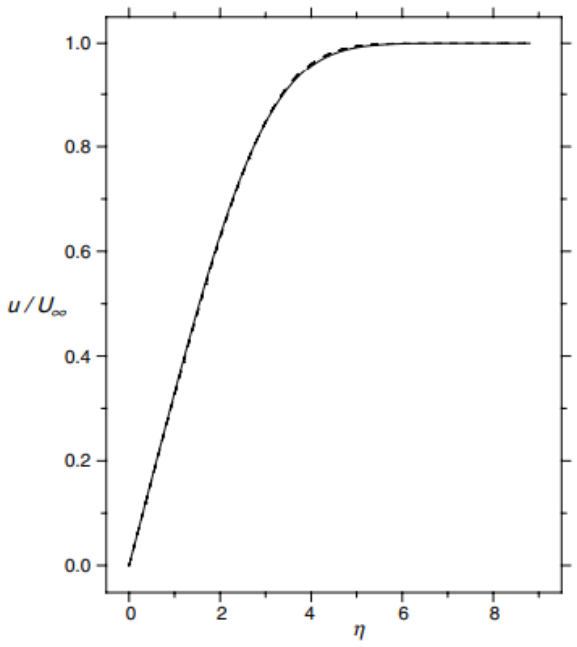

Fig. 3. A lower velocity profile parallel to the plate surface.

The Blasius solution is depicted by the solid line. Equivalent to the dashed line is a profile calculated using Equation (2).

Equation (2) gives us an approximation of velocity, which is shown in Fig. 3 as a dashed line alongside Blasius's result (the values used for rv and l1 are given below). Gaussian-like behaviour has been observed in a second derivative of the velocity because of the close proximity of these lines.

$$\mu_n \equiv \int_0^\infty dy(y-\mu_1)^n \frac{d^2\left\{-\mu_1\frac{u(y)}{U_\infty}\right\}}{dy^2} \quad (3)$$

3. SYSTEM CONFIGURATION

3.1 Computational fluid dynamics

An analysis tool for fluid flow, heat transfer, and other related processes, computational fluid dynamics (CFD) is a computer simulation. Numerical algorithms are used by these simulation tools to solve the relevant physical process. Numerical solution techniques include finite difference, finite element, and spectral methods, which are all distinct from one another. The CFD code chosen in this project, CFX, uses a special finite difference formulation called the finite volume method. How this works is that the user creates a computational grid on the domain consisting of cells (control volumes). For each control volume, the governing equations of fluid

flow are integrated, discretized into algebraic equations, and then solved using an algorithmic method. The complex and non-linear nature of the governing equations (equations (4) – (8)) necessitates an iterative approach.

$$Continuity: \frac{\partial \rho}{\partial t} + div(\rho u) = 0 \quad (4)$$

$$X - momentum: \frac{\partial(\rho u)}{\partial t} + div(\rho u \boldsymbol{u}) = -\frac{\partial p}{\partial x} + div(\mu\, grad\, u) + S_{Mx} \quad (5)$$

$$Y - momentum: \frac{\partial(\rho v)}{\partial t} + div(\rho v \boldsymbol{u}) = -\frac{\partial p}{\partial y} + div(\mu\, grad\, y) + S_{My} \quad (6)$$

$$Z - momentum: \frac{\partial(\rho w)}{\partial t} + div(\rho w \boldsymbol{u}) = -\frac{\partial p}{\partial z} + div(\mu\, grad\, w) + S_{Mz} \quad (7)$$

$$Energy: \frac{\partial(\rho i)}{\partial t} + div(\rho i \boldsymbol{u}) = -p\, div\, u + div(k_t\, grad\, T) + \Phi + S_i \quad (8)$$

The governing equations come from applying the three fundamental physical laws of conservation of mass, momentum and energy to a control volume. For further information about these laws, the derivation of the equations and the numerical approach used by CFX, the reader is referred to standard text books in fluid dynamics and CFD.

3.1.1 Turbulence modeling

The turbulent nature of flows makes them much more difficult to calculate than if they are laminar. Due to the random and chaotic nature of the turbulent flow, eddies have a wide range of length and time scales. This can be done by using direct numerical simulation (DNS), large eddy simulation (LES) and Reynolds-averaged Navier–Stokes equations (RANS) for turbulence modelling (RANS). Using the DNS method, four equations with four unknowns can be formed using the turbulent continuity and Navier-Stokes equations. These can then be used to find a starting point for the simulations, which then develops a transient solution to resolve all the scales of the motion. This method requires extremely fine computational grids (around 103 grid points in each coordinate direction) and very small time steps, which makes it too computational heavy to be used in industrial applications and hence it is more commonly used in fundamental research in turbulence.

The LES method uses a filtering method on the Navier-Stokes equations to separate the larger and smaller eddies. The larger eddies are then resolved using unsteady flow simulations while the smaller scale eddies are modeled with a so called sub-grid model. This method is much less demanding on computational resources than DNS but it still requires a lot more computer power than the third method.

3.2 Boundary layers

Consider fluid flow over a flat plate, like in Figure 4. Small velocity gradients and little friction affect the flow in the vast majority of the flow field away from the surface. At the wall however, the velocity gradients are large and friction has a large impact on the flow due to the frictional forces retarding the motion of the fluid, and hence a thin layer is formed above the surface. This thin viscous region is called the boundary layer. A no-slip condition occurs when flow velocity at the surface is equal to the freestream velocity, u∞. As we move away from the surface, flow velocity increases to the point where it equals the freestream velocity. The height and it's normallyδabove the wall where this occurs is called the boundary layer thickness defined as the point above the wall where the velocity equals 99 % of the freestream velocity (equation (9)).

$$u = 0.99u_{\infty} \quad (9)$$

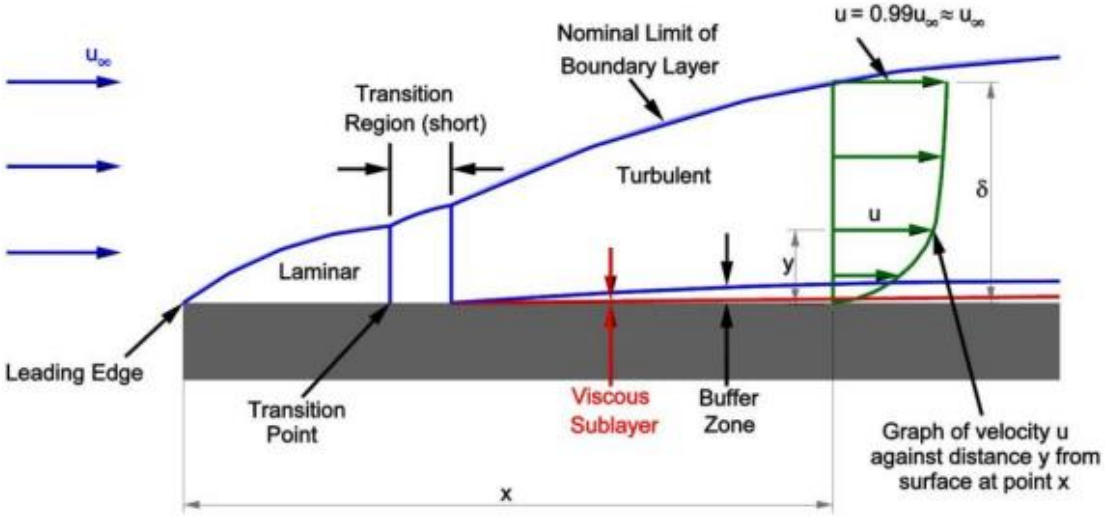

Figure 4: Boundary layer along a flat plate.

Boundary layers (BL) can be laminar or turbulent depending on the Reynolds number (Re). The flow over a flat plate changes from one to the other at approximately Re = 5*105. Lower Reynolds numbers are laminar, while higher Reynolds numbers are turbulent, and the velocity changes uniformly as one moves away from the wall in a straight line.

Particles of fluid in the BL do not always adhere to the body's surface in a thin layer along its length. The flow in the boundary layer can be reversed and the boundary layer's thickness can increase significantly when adverse pressure gradients are present. Because of reversed flow, there is a large wake of backwards-flowing water that separates from and recirculates the surface. This will cause a pressure drop in the region and will increase the pressure drag on the body.

4. METHODOLOGY

To validate the local non-conformance definition for the bumps the work was split up into several parts. First an investigation of the flow over a flat plate was conducted (reference case) to visualize the boundary layers and to find the thickness at a position where the flow was fully developed. This was done for Reynolds numbers ranging from 10^5 to 10^7 to see how the thickness changed with Re.

Since the NC definition that VAC use is defined as a percentage of the boundary layer thickness (BLT), bumps were created with a height of 10, 40, 60, 99 and 150 % of the BLTs found in the flat plate simulations. This was done to see how the size and shape of the BL was affected by the bumps. A correlation for the drag coefficient for the bumps was then derived based on the data from the bump analysis.

Finally the boundary layers for representative vanes of a TRF were analyzed for both nominal cases and with bumps so that VAC could be provided with recommended values for maximum allowed bump sizes on the vanes. The correlation derived from the flat plate simulations was then tested on some of the bump cases to see how well it predicted the drag coefficient.

4.1 Simulation approach

A similar approach was used during all the simulations to standardize the work. All the flat plate simulations were very much alike, apart from slight geometry changes and boundary conditions, which made it possible to keep a lot of things constant during the process. For each case the steps below were followed.

1. Create the geometry.

2. Create the computational grid. Depending on the inlet boundary condition used in step 3, modify the distance from the wall to the first node.

3. Define the simulation case with appropriate boundary conditions and simulation settings.

4. Run the calculations. Monitor convergence of the residuals and domain imbalances until the monitored parameters can be considered to be low enough and steady.

5. Check if the y + value fulfills the criteria demanded by the turbulence model. If it does, continue to step 6, otherwise repeat step 2-5.

6. Post-process the results.

4.1.1 Software and simulations settings

Due to the simple geometry of a flat plate it was constructed in the geometry builder of the meshing software ANSYS ICEM 12.1. The bumps that were to be placed on the flat plate were created in MATLAB and then imported as formatted point data files into ICEM. All the mesh generation was then done with ICEM.

The solver chosen was the commercial software package ANSYS CFX 12.1 where CFX-Pre was used for defining the simulations and CFX-Solver for running them. In CFX-Pre the simulations SST turbulence model. This were set up as steady and incompressible and run with the k- calculating the advection terms in the discrete finite volume equations as well as the turbulence numerics, 2nd order high resolution schemes were utilized. Since the boundary layers were studied in detail it was important to use a turbulence model that could utilize a fine mesh and SST model was chosen because of it advantages to calculate well and close to the walls.

The post-processing was carried out in several programs. CFX-Post was mainly used for exporting data from the CFD-simulations for the BL and drag coefficient calculations. MATLAB was utilized to deal with the large amount of data needed to calculate the boundary layer thickness and doing the BL calculations. Microsoft Excel was used for evaluating all the data relevant to the drag coefficient as well as deriving the correlation.

4.2 Boundary conditions

The leftmost side in Figure 5 was set as an inlet with a velocity Vin depending on the Reynolds number ReL wanted at a location of x = 19 meters (Table 1). VACs applications aren't restricted to just one Re so it was important to study how the BL changed with an increasing value, but also to be able to find a correlation that would work for a wide range of Re. The inlet velocity was calculated from equation (10).

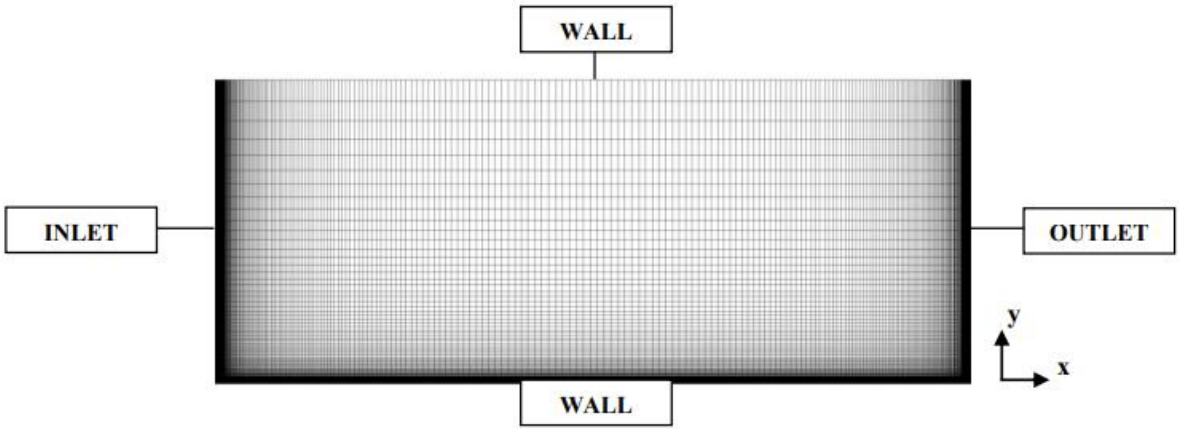

Figure 5: Initial 2D-mesh for the reference case.

$$Re_L = \frac{\rho_\infty V_\infty L}{\mu_\infty} \quad (10)$$

Table 1: Inlet velocities for different Reynolds numbers.

Re_L	V_{in} [m/s]
100'000	0.081
250'000	0.203
500'000	0.407
750'000	0.610
1'000'000	0.813
2'000'000	1.627
4'000'000	3.253
6'000'000	4.880
8'000'000	6.506
10'000'000	8.132

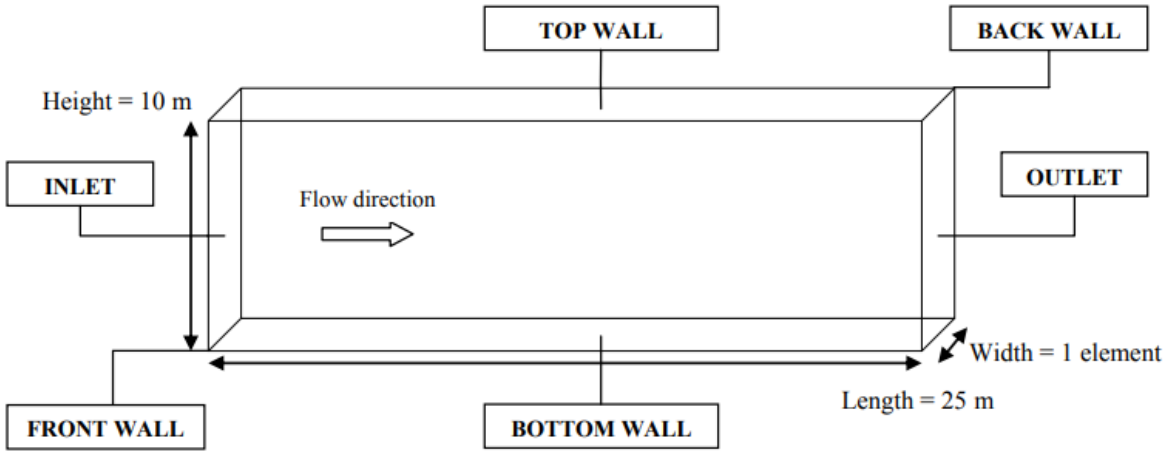

Figure 6: Reference case geometry: flat plate.

Using a wall with a no-slip boundary condition, the bottom side of the geometry was given the appearance of a plate.

The top side of the domain was set as a wall with a free-slip condition.

The two walls in the cross-flow direction (Figure 6) were both given a symmetry boundary condition (ANSYS Inc, Modeling 2D Problems, 2020).

For the rightmost side of the domain an outlet boundary condition was set with an average static pressure of zero Pascal over the whole outlet.

4.3 The Runge-Kutta Method for the Blasius Equation

The obtained third-order, nonlinear, ordinary differential equation cannot be solved analytically and has to be solved numerically. A technique that can be used is the Runge-Kutta method. The method integrates in small steps along the y-direction, starting from the wall.

However, because we only have two of the boundary conditions at y=0 (the boundary condition for $f''(0)$ is missing), we have to assume a value for this boundary condition and check if at large η, the condition $f'(\infty) = 1$ is satisfied. This process is repeated until the solution is congruent. This method is also called the 'shooting-method' and Matlab will provide the help needed to find the solution.

5. RESULTS AND DISCUSSION

5.1 Reference case

Following the method for calculating the BLT for the flat plate yielded the results shown in Figure 7. The line at the top of the graph is the lowest Re (10^5) and the bottom one the highest (10^7) and as was mentioned earlier they all correspond to a Re at 19 meters in the flow direction.

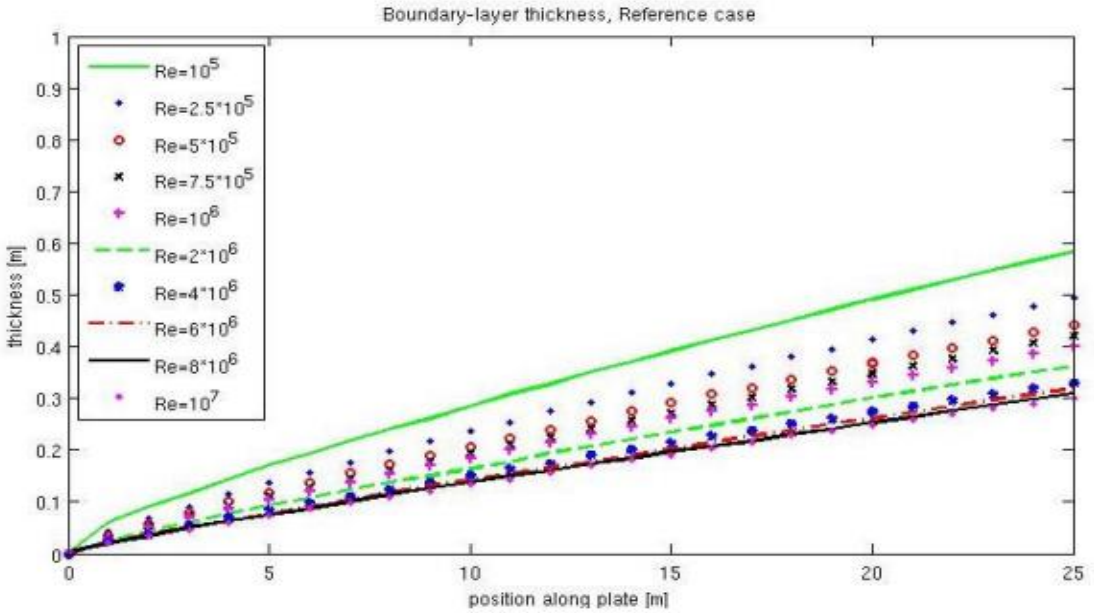

Figure 7: Boundary layer thickness for the reference case.

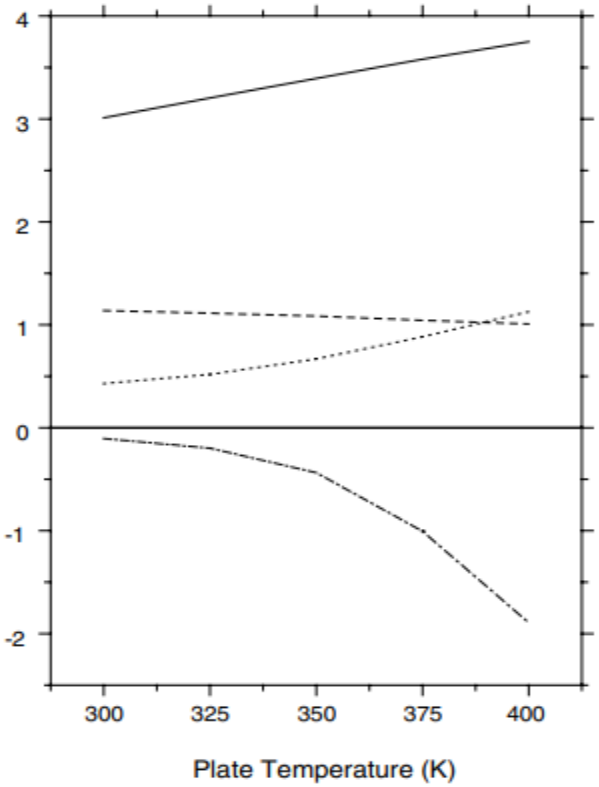

Fig. 8. The first two moments of the velocity boundary layer, the skewness, and the excess calculated as a function of plate temperature (T1 = 300 K, Re = 5000).

This flavour can also be found in the skewness and excess terms in the boundary layer context, but they tend to be biassed by the velocity profile near the plate. The calculated higher order moments, as shown in Fig. 8, are the most obvious examples of this behaviour.

5.2 Comparison analysis

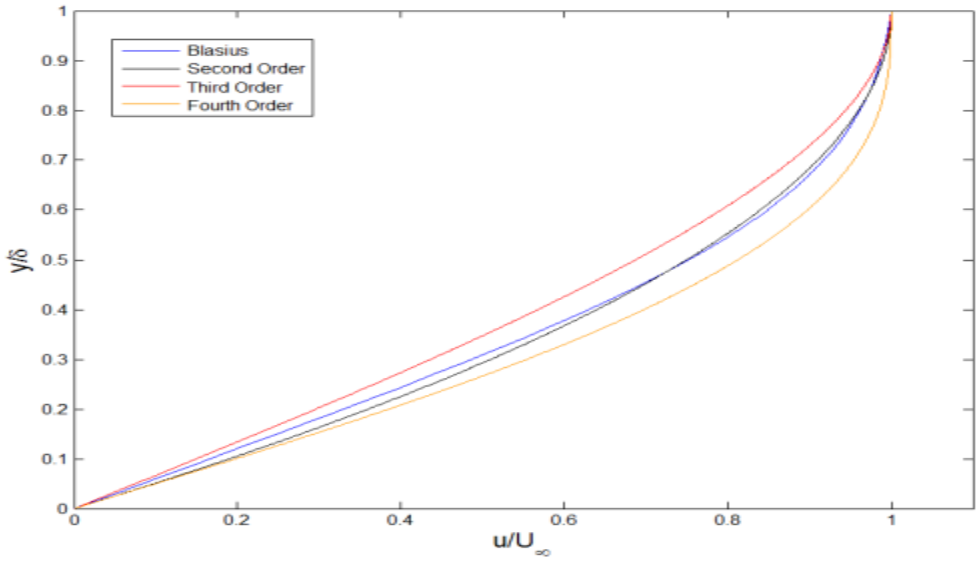

Figure 9: Comparison of the velocity profiles

In Figure 9, η is plotted against u/U∞ and the four velocity profiles are compared.

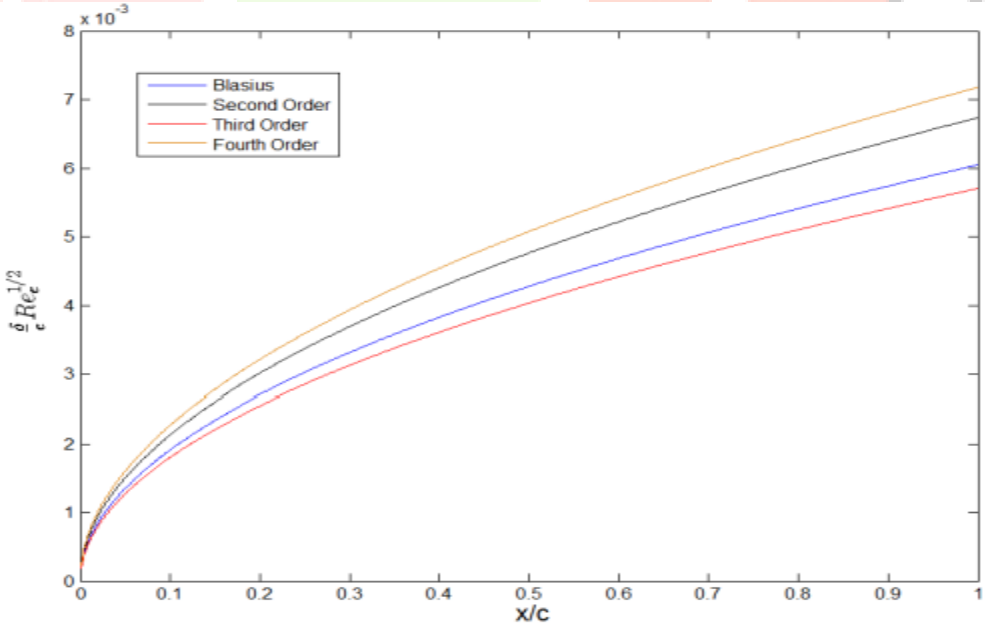

Figure 10: Comparison of the boundary-layer thickness.

Second-order approximation in Figure 10 is close to the Blasius solution. There is even more discrepancy between the Blasius equation and the fourth-order approximation in the boundary-layer thickness graph Here, the third-order approximation appears to be the most accurate.

CONCLUSION

It has been determined that the boundary layer thickness can be defined mathematically, along with a number of additional parameters that can be used to measure the behaviour of the velocity and temperature profiles. Experimental and computer-generated velocity and temperature profiles, as well as laminar and turbulent flow, should all be compatible with the method. It was studied both with and without bumps on the suction and pressure sides of real geometries that represent the vanes in the turbine rear frame. Boundary layer thicknesses at the suction peak on the regular vane and the mount vane were found to be 3.4 mm at 50% span on the regular vane and 3.1 mm at 90% span on the mount vane. It was extremely difficult to calculate the boundary layer thickness along the vanes when large bumps of more than 1 mm were present, as they were on both vane types. More than 80 percent increase in boundary layer thickness was found on regular vane and 20 percent on mount vane for bumps of 1 mm in diameter.

REFERENCES

1. Street, R.L. A linearized Theory for Rotational Super-Cavitating Flow. J. Fluid Mech. 1963, 17, 513–545. [CrossRef]

2. Vasiliev, V.N. Cavity vortex flow past a curved arc. In Unsteady Motion of Bodies in Liquid; University of Chuvashia: Cheboksary, Russia, 1979; pp. 3–15.

3. Kotlyar, L.M.; Lazarev, V.A. Cavity vortex flow past a wedge. In Proceedings of the Boundary-Value Problem Workshop; Kazan' State University: Kazan, Russia, 1971; pp. 15–25.

4. Sedov, L.I. Plane Problems in Hydrodynamics and Aerodynamics; Nauka: Moscow, Russia, 1980; p. 448. (In Russian)

5. Muskhelishvili, N.I. Singular Integral Equations: Boundary Problems of Function Theory and Their Applications to Mathematical Physics; Dover Publ.: New York, NY, USA, 1992.

6. Burov, A.V. Uniformly Whirling Jet Flow Past a Wedge. In High-Speed Hydrodynamics; University of Chuvashia: Cheboksary, Russia, 1985; pp. 22–24.

7. Yoon, B.S.; Semenov, Y.A. Cavity flow in a boundary layer. In Proceedings of the 26th International Conference on Offshore Mechanics and Arctic Engineering (OMAE), Shanghai, China, 6–11 June 2010.

8. Brillouin, M. Les surfaces de glissement de Helmholtz et la resistance des fluids. Ann. Chim. Phys. 1911, 23, 145–230.

9. Villat, H. Sur la validite des solutions de certains problemes d'hydrodynamique. J. Math. Pure Appl. 1914, 20, 231–290.

10. Arakeri, V.H.; Acosta, A.J. Viscous effects in the inception of cavitation on axisymmetric bodies. Trans. ASME J. Fluids Engng. 1973, 95, 519–527. [CrossRef]

11. Arakeri, V.H. Viscous effects on the position of cavitation separation from smooth bodies. J. Fluid Mech. 1975, 68, 779–799. [CrossRef]

12. Tassin Leger, A.; Ceccio, S.L. Examination of the flow near the leading edge of attached cavitation. Part 1. Detachment of two-dimensional and axisymmetric cavities. J. Fluid Mech. 1998, 376, 61–90. [CrossRef]

13. Yoon B.S.; Semenov, Y.A. Cavity detachment on a hydrofoil with the inclusion of surface tension effects. Eur. J. Mech. B/Fluids 2011, 30, 17–25. [CrossRef]

14. Michell, J.H. On the theory of free stream lines. Philos. Trans. R. Soc. Lond. A 1890, 181, 389–431. [CrossRef]

15. Joukovskii, N.E. Modification of Kirchhof's method for determination of a fluid motion in two directions at a fixed velocity given on the unknown streamline. Math. Sbornik. 1890, 15, 121–278.